Numerical Simulator for the Coupled Model of Wells and Fractured Reservoirs

Mitsuo Matsumoto[1], Naoto Yoshida[2], Tsukasa Higuchi[2] and Keitaro Takaki[2]

[1] Department of Earth Resources Engineering, Faculty of Engineering, Kyushu University

744, Motooka, Nishi-ku, Fukuoka 819-0395, Japan

[2] Department of Earth Resources Engineering, Graduate School of Engineering, Kyushu University

744, Motooka, Nishi-ku, Fukuoka 819-0395, Japan

matsumoto@mine.kyushu-u.ac.jp

Keywords: *wellbore flow simulation, reservoir simulation, cycling wells*

ABSTRACT

This study presents a numerical simulator for the coupled model of wells and reservoirs, which is being developed. The simulator is capable of transient flows along directional wells and intersecting multiple planar structures based on the concept of discrete fracture network models. Comparisons with analytical and numerical solutions obtained using reference codes successfully validated the simulator of this study. An application to the hypothetical coupled problem of a directional production well intersecting multiple planar structures was demonstrated, in which a steam cap was generated at the top of the reservoir while producing for 300 days. The flowing enthalpy at the wellhead varied depending on the temporal variation in the flow rate in each feed zone. The simulator will be further extended and enhanced based on the requirements of specific problems and suggestions from scholars in open communities.

1. INTRODUCTION

An adequate understanding of the coupled flows between wells and reservoirs is key to efficiently design and optimize geothermal power plant facilities. Therefore, several efforts to understand wellbore flow by numerically reproducing and forecasting have been made and achieving successful implementations and applications (Miller, 1980; Pritchett, 1985; Aunzo et al., 1991; García-Valladares et al., 2006; Pan and Oldenburg, 2014; Tonkin et al., 2023a,b). Owing to the significant difference in temporal and spatial scales between transient flows in and around a wellbore and the entire reservoir, fully coupled numerical modeling of these flows has been a challenging problem.

This paper presents the specifications, validations, and hypothetical application of a simulator for this problem that is currently in development. The motivation to develop this simulator originated in extending the code for the transient wellbore flow model presented by Matsumoto et al. (2021, 2023). Matsumoto et al. (2021) derived an empirical equation that depicted the boundary between the conditions generating constant and periodic wellbore flows through exhaustive numerical experiments. The equation was based on the mean specific enthalpy of the shallow and deep reservoirs, intersected by a production well, weighted by their productivity indices. Matsumoto et al. (2023) extended the equation to take into account the dependence on reservoir pressures. A highly simplified reservoir model was attached to their wellbore model, assuming steady-state radial flow with uniformly constant specific enthalpy distribution in a disk-shaped horizontal reservoir. By replacing the reservoir model, we intend to validate the applicability of the empirical equation to further practical conditions of transient non-isenthalpic flow in inclined planar reservoirs. The inclination potentially generates a steam cap along with pressure decline and downflow of low-enthalpy injected fluid due to gravitational effects as well as intersections and connections between planar reservoirs.

The simulator can simulate transient flows along directional wells with multiple feed zones. Based on the concept of discrete fracture network models, wells can intersect multiple planar structures that are flexibly distributed and form a reservoir. In particular, we intend to implement a combination of steady-state wellbore flow simulation and the empirical equation to determine the stability of wellbore flow in practical production and reinjection problems. This will significantly reduce computational load by avoiding transient wellbore flow simulations. The simulator is currently capable of fundamental mathematical models and functions and will be continuously extended and enhanced based on the requirements of specific problems and suggestions from scholars in open communities.

2. OUTLINE OF THE SIMULATOR

The simulator, written in Fortran to maximize computational performance, was primarily designed to represent geothermal reservoirs, consisting of multiple planar permeable structures, such as fractures, permeable layers, and formation boundaries, distributed three-dimensionally. Directional wells can be connected to planar permeable structures at multiple intersections. Transient flows along the wells and planar permeable structures are fully coupled by generating and solving a unified nonlinear system with respect to the primary variables defined at each numerical cell or grid point.

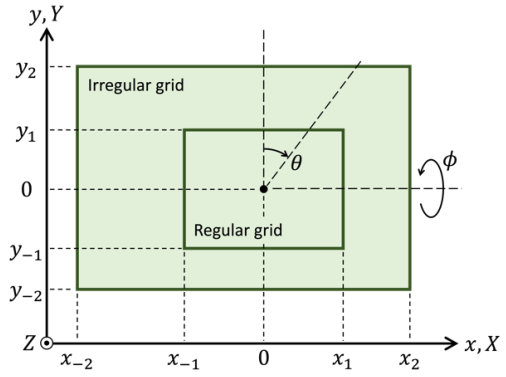

Figure 1: Planar structure set at the default position. The local coordinates (x, y) correspond to the global coordinates $(X, Y, 0)$. The direction of the planar structure is defined by the dip ϕ and azimuth θ.

Proceedings 45th New Zealand Geothermal Workshop
15-17 November, 2023
Auckland, New Zealand
ISSN 2703-4275

2.1 Model Structure

2.1.1 Planar structure

Each rectangular planar structure has a local Cartesian coordinate system (x, y) defined individually (Figure 1), in addition to the global Cartesian coordinate system (X, Y, Z) covering the total model. To define the dimensions and numerical grid sizes in the x- and y-direction of a planar structure, users specify the coordinates $x_{\pm1}$, $x_{\pm2}$, $y_{\pm1}$, and $y_{\pm2}$. The external boundaries of the planar structure are at $x = x_{\pm2}$ and $y = y_{\pm2}$. Obeying the grid indices specified by the users, an exponentially expanding irregular grid is generated in the outer region, while a regular grid is generated in the inner region restricted by the coordinates $x_{\pm1}$ and $y_{\pm1}$. The direction of the planar fracture is specified by rotating in the ϕ-direction (dip) from the default position shown in Figure 1, followed by rotation in the θ-direction (azimuth). The planar fracture is subsequently located at an arbitrary position in the global coordinate system by specifying the correspondence between the local origin $(x, y) = (0,0)$ and the global coordinates. The intersections between the planar fractures are automatically detected and determined to construct a unified three-dimensional numerical grid.

2.1.2 Well and interface

The trajectory and numerical grid for each well in the global coordinate system are determined in two phases. In the first phase, the list of inclination and azimuth angles at each drilling depth and the global coordinates at the wellhead are referenced to determine the trajectory and define a regular one-dimensional numerical grid. In the following phase, the trajectory and numerical grid are modified to be consistently connected to planar structures because the grid points in a well and planar structure must coincide at each intersection. When the numerical grid for a well is automatically modified by searching for and connecting adjacent grid points, the well trajectory will unacceptably change if the numerical grids for the planar structures are insufficiently refined. The numerical grid along the well is no longer regular after the modification.

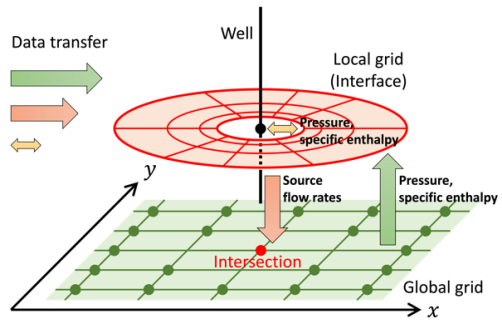

Figure 2: Schematic flow of data transfer among the global and local grids for a planar structure and the grid for a well. The black and red circles coincide and denote the intersection between the well and planar structure. The data at the green circles in the global grid are referenced by the local grid.

At each intersection between the well and planar structure, a ring-shaped local grid overlapping the planar fracture was applied, which provided an interface between the well and planar structure to accurately simulate temporal and spatial variations in the vicinity of the wellbore (Figure 2). The external radius of the local grid, which obeys the polar coordinate system, is defined by the double spacing of the global grid, covering the total planar structure, whereas the internal radius is restricted by the wellbore radius. At the external boundary, the local grid references the values of the primary variables (i.e., pressure and specific enthalpy) stored in the global grid using the bilinear interpolation method. At the internal boundary, the local grid and grid for the well share the values of the primary variables by referring to each other. The mass and enthalpy flow rates between the planar structure and well determined using the local grid are exported to the source terms of the mass and energy conservation equations solved in the global grid. Thus, the transient flows in the wells, planar structures (global grid), and the interface between them (local grid) are dynamically simulated by referring to each other in real time using a unified three-dimensional grid.

2.2 Mathematical Model and Numerical Techniques

2.2.1 Governing equations

The simulator is currently capable of simulating the coupled transient flow of pure water in wells and planar structures under two-phase and nonisothermal conditions without heat loss across the wellbore and planar surfaces. Mass and energy conservations in the planar structures obey the expressions employed by the reservoir simulator TOUGH2 (Pruess et al., 1999). The mass flux obeys Darcy's law for a two-phase flow, considering the relative permeabilities of both phases. The mass and energy balances in each numerical cell are restricted by flows over multiple planar structures through intersections as well as flows within a single planar structure. The source terms of the conservation equations refer to the flow rates between the well and interface (Figure 2). The conductive heat flux is assumed to be negligible. The thermodynamic properties and viscosity of water are computed using the equation of state IAPWS-IF97 (IAPWS, 2007) and an empirical equation (IAPWS, 1997), respectively, developed by the Internal Association for the Properties of Water and Steam (IAPWS).

For the wells, the homogeneous flow model, neglecting the slip between liquid and vapor phases, presented by Matsumoto et al. (2021) is assumed to successively extend the conditions of their model. Future studies should employ more sophisticated models, such as the slip and drift-flux models, as Tonkin et al. (2021) reviewed extensively. Based on exhaustive review and evaluation, Tonkin et al. (2023a,b) recently presented an advanced transient wellbore flow simulator employing one of the suitable drift-flux models (Shi et al., 2005) and demonstrated applications to several challenging problems: opening and closing wells, a completion test, air lifting and compression, and injection of water-carbon dioxide mixtures. Conditions for generating periodic wellbore flow based on the homogeneous flow model, which we currently focus on, will provide a basis to understand the mechanism of periodicity when the model is extended to those taking into account the slip.

By discretizing the governing equations for the planar structures, including the interface, and those for the wells using the integral finite difference method in a unified three-dimensional grid, which has N cells or grid points in total, we obtain and solve a nonlinear system with $3N$ unknowns and equations at each time step because we have three primary variables at each cell or grid point: pressure, specific enthalpy, and tracer concentration in planar structures; and pressure, specific enthalpy, and flow velocity in wells. The

tracer concentration is currently inactivated by assuming a uniform constant value. The nonlinear system is numerically solved using the Newton–Raphson method. The linear system appearing in every iteration of this method is solved using the biconjugate gradient-stabilized method with the preconditioner of incomplete LU decomposition.

2.2.2 Initial and boundary conditions

The initial one-dimensional distributions of pressure and specific enthalpy in planar structures are determined based on user indications in the global grid. The initial specific enthalpy distribution is determined by interpolating and extrapolating the specified values to an arbitrary number of reference elevations (Z). With respect to the initial specific enthalpy distribution, the initial pressure obeys a hydrostatic distribution based on a specified value at the reference elevation. Referring to the initial condition in the global grid determined in advance, the initial condition over a well and local grid is determined by assuming a steady-state flow with a specified wellhead condition, as presented by Matsumoto et al. (2021).

For each external boundary of planar structures ($x = x_{\pm 2}$ or $y = y_{\pm 2}$ in Figure 1), the boundary condition can be selected from three options: impermeable and insulated condition, fixed-state condition at the initial values, and quasi-infinite-acting condition. The quasi-infinite-acting condition is implemented by assuming sufficiently large absolute values of $x_{\pm 2}$ or $y_{\pm 2}$, compared with the simulation period of specific problems so that boundary effects will not appear before the simulation runs finish. The boundary condition at each wellhead is selected from two options: known wellhead pressure or flow rate. The specific enthalpy of the fluid must also be specified during injection.

3. VALIDATIONS

3.1 Line-Source Problem

The line-source problem, assuming production at a constant flow rate using a vertical well with a negligible diameter intersecting a planar horizontal reservoir, was simulated to validate the simulator by comparing it with an analytical solution. We assumed a pair of intersecting planar structures, equivalent to a single square planar structure with a side length of 20 km, in terms of pressure variations (Figure 3). Assuming this condition, we intended to validate the connection between the planar structures. The total number of cells or grid points was 920, including the global and local grids. The reference pressure for the initial hydrostatic distribution was 12 MPa at the elevation of the horizontal planar structure, and the initial specific enthalpy was uniform at 500 kJ/kg, which indicated a liquid-dominated reservoir. Impermeable and insulated conditions were assumed at all external boundaries of the planar structures. The permeability–thickness and porosity–thickness products were 1.0×10^{-11} m^3 and 1.0 m, respectively. The thickness of the planar structure was assumed to be 10.0 m, which resulted in a porosity of 10%. The volumetric heat capacity of the rock matrix was 2.6×10^6 J/m^3/K. Production at a constant rate of 10 t/h for 100 days using an 8.5-inch production well, intersecting one of the planar structures at a point 10 km from each external boundary, was assumed, which was able to be reproduced using the combined global and local grids without a well model.

The temporal pressure variation at the internal boundary of the local grid on a logarithmic scale successfully reproduced the analytical solution assuming an infinite-acting condition (Theis, 1935) (Figure 4a). The instant at which the numerical solution began to diverge from the straight line of the analytical solution consistently corresponded to the radius of investigation, reaching an external boundary 10 km from the well. After diverging from the analytical solution, the temporal variation exhibited a straight line on a linear scale, which was consistent with the impermeable external boundary condition. The spatial pressure variation was consistent with that of the analytical solution (Figure 4b). The spacing in the local grid expanded exponentially from 10 mm at the internal boundary to 374 m at the external boundary, which successfully reproduced a steep pressure drop in the vicinity of the wellbore.

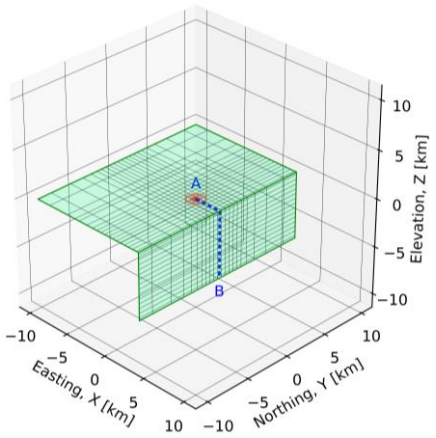

Figure 3: Planar structures forming the model for the line-source problem, consisting of global (green) and local (red) grids, drawn by cell boundaries. The spatial pressure variation in Figure 4 is along Line AB from the internal boundary of the local grid to the external boundary of the global grid.

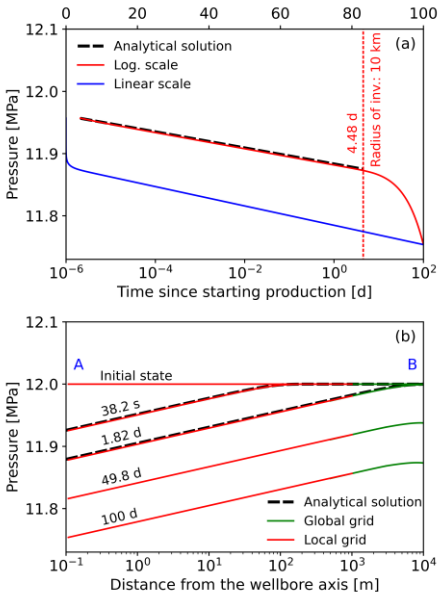

Figure 4: Comparison between the numerical solution of this study and the analytical solution (Theis, 1935) for the line-source problem: (a) temporal pressure variation at the internal boundary of the local grid

ISSN 2703-4275

and (b) spatial pressure variation along Line AB in Figure 3.

3.2 Generation of a Steam Cap

A steam cap generated at the top of a vertical planar reservoir owing to a pressure decline was reproduced to validate the simulator of this study by comparing it with the reservoir simulator TOUGH2. We assumed a vertical square planar structure with a side length of 2000 m. The reference pressure for the initial hydrostatic distribution was 19.35 MPa at 525 m from the bottom, and the initial specific enthalpy distribution was assumed to generate a uniform temperature distribution at 140.8℃. Impermeable and insulated conditions were assumed for all the external boundaries. The permeability–thickness and porosity–thickness products were 1.0×10^{-11} m^3 and 0.1 m, respectively. The thickness of the planar structure was assumed to be 1.0 m, which resulted in a porosity of 10%. The volumetric heat capacity of the rock matrix was 2.6×10^6 $J/m^3/K$. For simplicity, linear relative permeability functions with no residual saturations were assumed for both phases. The production rate was maintained at a rate of 10 t/h for 300 days using a point source located at 525 m from the bottom and one of the side boundaries. A global grid covering the total reservoir was applied without a local grid and well model. The total number of cells or grid points was 1444.

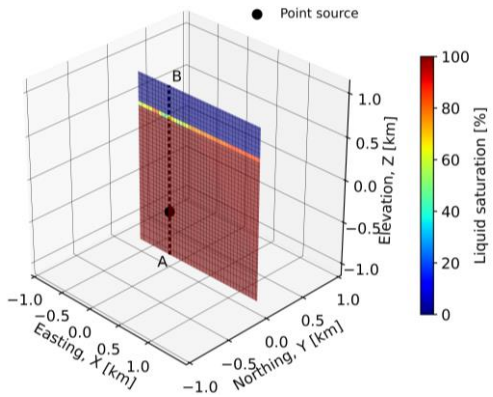

Figure 5: Distribution of liquid saturation superimposed on cell boundaries after production at the point source for 300 days reproduced using the simulator of this study. The profiles of pressure and liquid saturation along Line AB are shown in Figure 7.

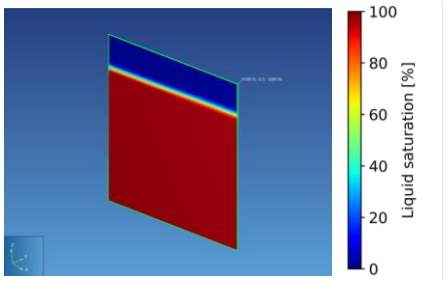

Figure 6: Distribution of liquid saturation after production at the point source for 300 days reproduced using TOUGH2. The dimension of the planar reservoir is the same as that in Figure 5.

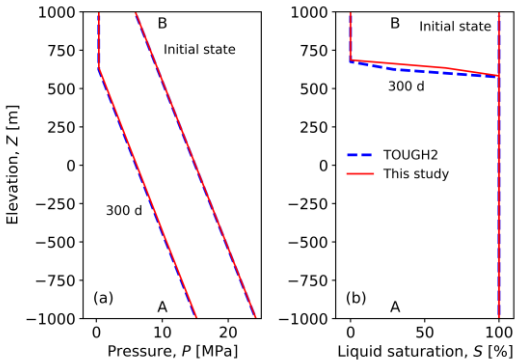

Figure 7: Profiles of (a) pressure and (b) liquid saturation along Line AB in Figure 5 reproduced using the simulator of this study and TOUGH2.

The generation of a steam cap reproduced using the simulator of this study was consistent with that reproduced using TOUGH2 (Figures 5–7), which successfully validated the two-phase flow and transition among the subcooled water, saturated water and steam, and superheated steam. Through production and subsequent pressure decline for 300 days, a steam cap appeared at the top of the initially liquid-dominated reservoir.

3.3 Downflow of Low-Enthalpy Fluid

By modifying the conditions of the previous problem, the downflow generated by injecting a low-enthalpy fluid was reproduced and compared with the numerical solution obtained using the reservoir simulator TOUGH2. The vertical dimension of the planar reservoir was reduced from 2000 to 1975 m to locate the top grid points along the top boundary, where the fixed-state boundary condition was assumed without modifying the cell layout of the model using TOUGH2. In the simulator of this study, the grid points were located on the external boundary of the planar structures, regardless of the boundary conditions, by assigning halved cells. The bottom and side boundaries were impermeable and insulated, as in the previous problem. Fluid with a specific enthalpy of 300 kJ/kg was continuously injected at a rate of 10 t/h for 3.0 years.

The downflows reproduced using both simulators were consistent (Figures 8–10). After the low-enthalpy fluid reached the bottom of the planar reservoir, the region with relatively low temperatures expanded in the horizontal direction along with the lateral flow. The heat transfer owing to advection under a gravity field reproduced using the simulator of this study was successfully validated. The slight differences between the temperatures at the bottom reproduced using the two simulators can be attributed to the difference in the numerical expression of the boundary conditions.

ISSN 2703-4275

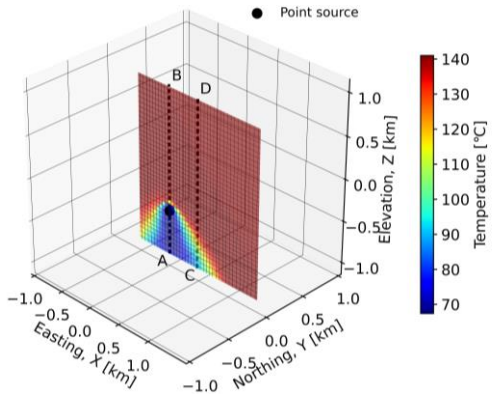

Figure 8: Temperature distribution superimposed on cell boundaries after injection at the point source for 3.0 years reproduced using the simulator of this study. The temperature profiles along Lines AB and CD are shown in Figure 10.

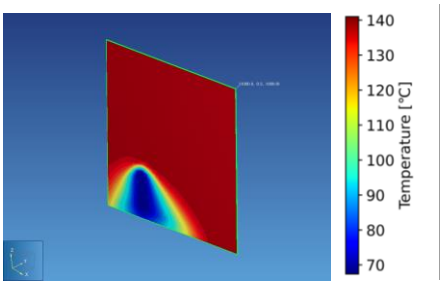

Figure 9: Temperature distribution after injection at the point source for 3.0 years reproduced using TOUGH2. The dimension of the planar reservoir is the same as that in Figure 8.

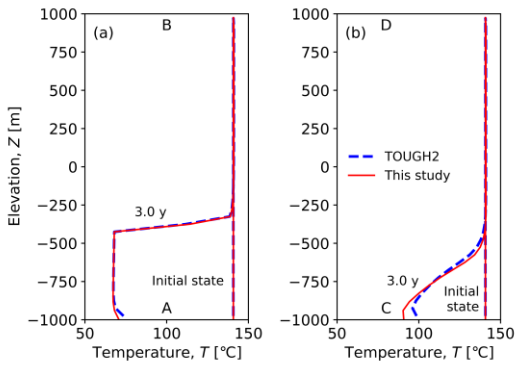

Figure 10: Temperature profiles along (a) Line AB and (b) Line CD in Figure 8 reproduced using the simulator of this study and TOUGH2.

3.4 Periodic Wellbore Flow

The periodic wellbore flow presented by Matsumoto et al. (2021) was reproduced to validate the simulator of this study. A vertical well with an inner diameter of 0.2 m was assumed to intersect the center of two planar and circular reservoirs at a depth of 1400 m and bottom of 2000 m (Figure 11). The pressure distributions in both reservoirs obeyed a steady-state solution based on the feed zone and external boundary pressures, whereas the specific enthalpies were uniformly constant. The external boundary pressure of the shallow and deep reservoirs was constant at 4.5 and 10.0 MPa, respectively. The specific enthalpy of the shallow reservoir varied from 764.9 kJ/kg (180°C) to 1037.7 kJ/kg (240°C), depending on the case. The specific enthalpy of the deep reservoir was commonly 1134.8 kJ/kg (260°C). The permeability–thickness product of the shallow and deep reservoirs was 4.0×10^{-12} and 1.0×10^{-12} m^3, respectively. The thickness of each reservoir was 1.0 m, which was restricted by the well grid size. Linear relative permeability functions with no residual saturations were assumed for both phases. The wellhead pressure was maintained at 0.7 MPa. The roughness involved in the frictional pressure loss in the wellbore was assumed to be 4.78×10^{-2} mm.

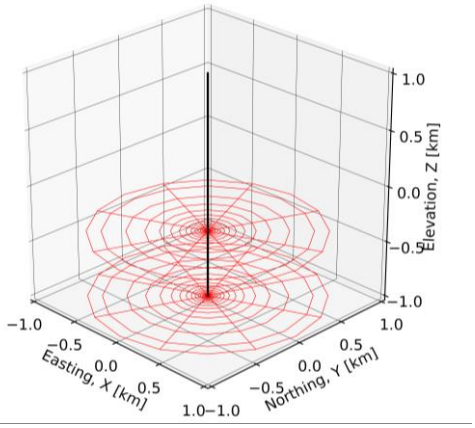

Figure 11: Vertical well intersecting planar structures forming the model for the periodic wellbore flow problem, consisting of a one-dimensional grid (black) for the well and local grids (red) for the circular reservoirs, drawn by cell boundaries. Global grids were inactivated.

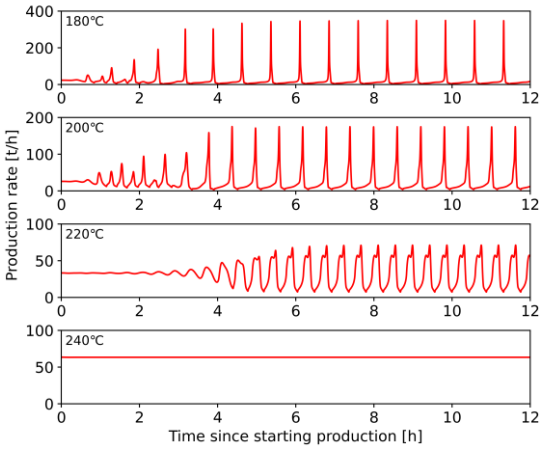

Figure 12: Temporal variations in production rates under four shallow reservoir temperatures reproduced using the simulator of this study. Reference simulations under equivalent conditions were presented by Matsumoto et al., (2021, Fig. 3).

Each circular reservoir was represented by a local grid with a fixed-state external boundary. The grid spacing in the local grid expanded exponentially from 1.0 mm at the internal boundary to 263 m at the external boundary, whereas that in

ISSN 2703-4275

the well was uniform at 1.0 m. The total number of cells or grid points was 2818, including the well and local grids. The initial state was determined by assuming steady-state flow over the well and reservoirs. The simulator of this study successfully reproduced the temporal variations in the production rates under four shallow reservoir temperatures, as presented by Matsumoto et al. (2021) (Figure 12).

Despite valid numerical solutions, the simulations of transient, in particular periodic, wellbore flows require extremely short time step sizes of a few seconds, which will result in unrealistic execution times when simulating practical production and reinjection problems, assuming multiple wells in actual fields. We aim to overcome this issue by combining steady-state wellbore flow simulation and an empirical equation to determine the stability of the wellbore flow. Figure 13 compares the production rates (mass flow rates at the wellhead) and mass flow rates in both feed zones between the transient and steady-state simulations of the problem described herein. The flow rates of the transient simulations were determined by averaging with respect to time from 6.0 to 12.0 h, during which stable periodic flows were established (Figure 12), whereas those of the steady-state simulations were from the initial state of the transient simulations. The steady-state simulations provided an approximation of the production rates and feed zone flow rates with sufficient accuracy for practical applications. To determine the stability, an extended empirical equation based on the mean specific enthalpy of shallow and deep reservoirs weighted by their productivity indices was derived and presented by Matsumoto et al. (2023), which depended on the pressures and specific enthalpies of the shallow and deep reservoirs. Future studies should apply a combination of steady-state simulation and an empirical equation to determine the stability of wellbore flow for further practical problems.

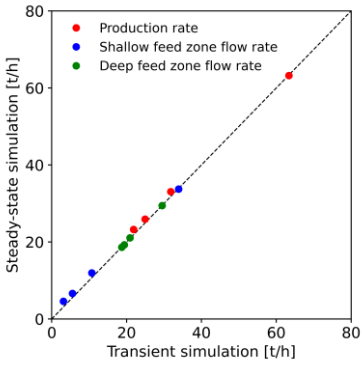

Figure 13: Comparison of production rates (mass flow rates at the wellhead) and mass flow rates in shallow and deep feed zones between the transient and steady-state simulations. The values for transient simulations are averages with respect to time from 6.0 to 12.0 h.

4. APPLICATION

Finally, we demonstrated an application to the hypothetical coupled problem of a directional well intersecting a reservoir consisting of multiple planar structures (Figure 14). We assumed three square planar structures with a side length of 1200 m, intersecting and connected obliquely to demonstrate the flexibility of the numerical grid. The reference pressure for the initial hydrostatic distribution was 10 MPa at an elevation of 0 m. A linear initial distribution of specific enthalpy with respect to elevation was assumed, referring to 1134.1 and 767.8 kJ/kg at elevations of −1000 m and 1000 m, respectively, and impermeable and insulated conditions were assumed at all external boundaries. The permeability–thickness and porosity–thickness products were 1.0×10^{-12} m^3 and 5.0 m, respectively. The thickness of the planar structure was assumed to be 50 m, which resulted in a porosity of 10%. The volumetric heat capacity of the rock matrix was 2.0×10^6 $J/m^3/K$. Linear relative permeability functions with no residual saturations were assumed for both phases.

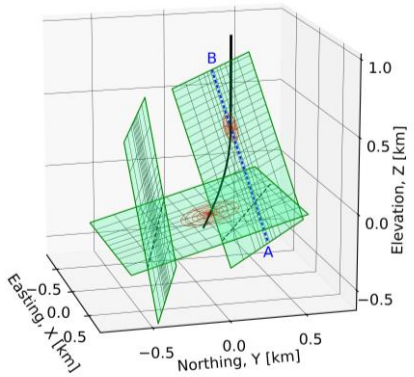

Figure 14: Directional well and planar structures forming the model for the hypothetical coupled problem, consisting of a one-dimensional grid (black) for the well and global (green) and local (red) grids for the planar structures, drawn by cell boundaries. The spatial variations in Figure 16 are along Line AB.

A directional well with inclinations up to 30° and a bottom drilling depth of 1300 m intersected the planar structures at the two intersections, forming shallow and deep feed zones at drilling depths of 611 and 1201 m, respectively. The inner diameter of the well changed stepwise at 500 m because of the 9-5/8-inch casing pipes and 7-inch slotted liner casing pipes. Production at a constant wellhead pressure of 0.5 MPa continued for 300 days. The total number of cells or grid points was 2215, including the well, local, and global grids.

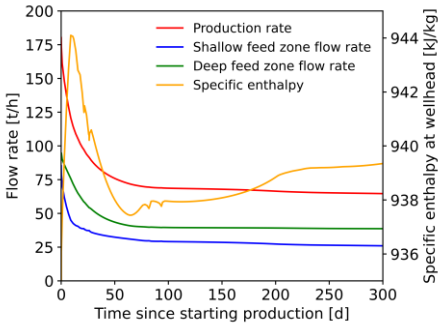

Figure 15: Temporal variations in a production rate and flowing specific enthalpy at the wellhead and mass flow rates at the shallow and deep feed zones.

The production and feed zone flow rates initially decreased, followed by a stable and slight decline after 100 days (Figure 15). The flowing specific enthalpy at the wellhead varied depending on the variation in each feed zone flow rate. The

ISSN 2703-4275

flowing specific enthalpies in the shallow and deep feed zones decreased slightly from 880 and 983 kJ/kg to 876 and 982 kJ/kg, respectively, within 300 days, owing to the downward migration of fluids with relatively low specific enthalpies. The decline in the reservoir pressure generated a steam cap and two-phase flow zone in the vicinity of the shallow feed zone (Figure 16). The wellbore flow simulated using the transient model did not exhibit periodicity throughout the simulation period. The flash point initially appeared at a drilling depth of 748 m and moved downward to 936 m because of the decline in reservoir pressure over 300 days (Figure 17).

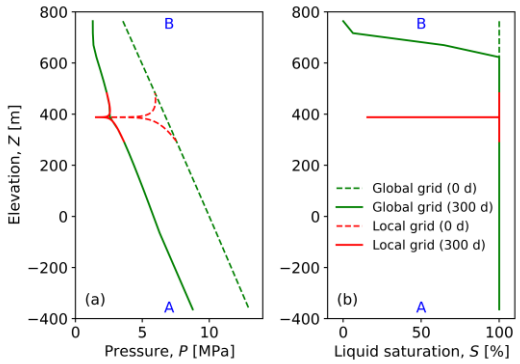

Figure 16: Spatial variations in (a) pressure and (b) liquid saturation along Line AB in Figure 14 simulated using the global and local grids. The initial distribution of liquid saturation was uniform at 100%.

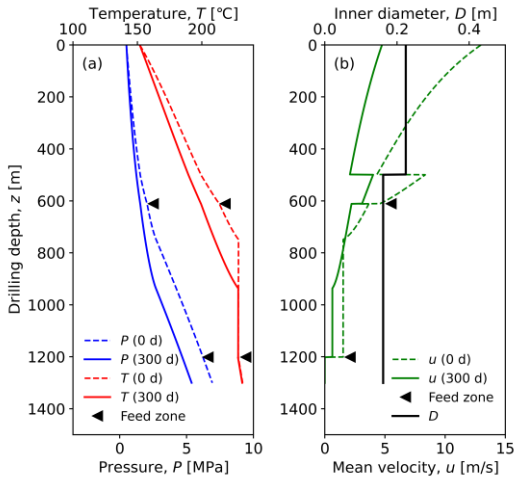

Figure 17: Profiles of (a) pressure and temperature and (b) mean velocity for both phases and inner diameter along the well intersecting the reservoir at two feed zones.

5. CONCLUSION

The simulator, which is under development and capable of simulating coupled transient flows along directional wells and multiple planar structures forming reservoirs, was validated by comparing with analytical and numerical solutions obtained using the reference codes. The simulator successfully reproduced the temporal and spatial variations in pressure for the line-source problem, the generation of a steam cap and low-enthalpy downflow in a vertical planar reservoir, and a periodic wellbore flow. Its application to the hypothetical coupled problem of a directional production well intersecting a reservoir consisting of multiple planar structures was successfully demonstrated.

Future studies should continuously extend and enhance the simulator based on the requirements of specific problems and suggestions from scholars in open communities. In particular, we intend to implement a combination of steady-state wellbore flow simulation and an empirical equation to determine the stability of the wellbore flow. This feature enables to evaluate the stability within an acceptable computational load by avoiding transient simulation while simulating practical production and reinjection problems in actual fields.

ACKNOWLEDGEMENTS

We thank the reviewers for several constructive and helpful comments to improve this paper significantly. This study was partially based on the results obtained from the project JPNP21001, commissioned by the New Energy and Industrial Technology Development Organization (NEDO). This study was partially supported by the JSPS KAKENHI (Grant Number JP20K05402).

REFERENCES

Aunzo, Z.P., Bjornsson, G., Bodvarsson, G.S., (1991). Wellbore models GWELL, GWNACL, and HOLA. Lawrence Berkeley Laboratory Report LBL-31428.

García-Valladares, O., Sánchez-Upton, P., Santoyo, E., (2006). Numerical modeling of flow processes inside geothermal wells: An approach for predicting production characteristics with uncertainties. *Energy Conversion and Management 47*, 11–12, pp.1621–1643.

International Association for the Properties of Water and Steam (IAPWS), (1997). Revised release on the IAPS formulation 1985 for the viscosity of ordinary water substance. IAPWS, 15 p.

International Association for the Properties of Water and Steam (IAPWS), (2007). Revised release on the IAPWS industrial formulation 1997 for the thermodynamic properties of water and steam. IAPWS, 49 p.

Matsumoto, M., Itoi, R., Fujimitsu, Y., (2021). Theoretical study of conditions for generation of periodic wellbore flow due to inflow of a lower-enthalpy fluid. *Geothermics 89*, 101948.

Matsumoto, M., Okada, H., Itoi, R., Fujimitsu, Y.: Numerical simulation of periodic wellbore flow due to inflow of low-enthalpy fluid. *Proc. 48th Workshop on Geothermal Reservoir Engineering*, Stanford, CA, United States. (2023).

Miller, C.W., (1980). WELBORE user's manual. Lawrence Berkeley Laboratory Report LBL-10910.

Pan, L., Oldenburg, C.M., (2014). T2Well—An integrated wellbore–reservoir simulator. *Computers & Geosciences 65*, pp. 46–55.

Pritchett, J.W., (1985). WELBOR: A computer program for calculating flow in a producing geothermal well. S-Cubed Report SSS-R-85-7283.

Pruess, K., Oldenburg, C., Moridis, G., (1999). TOUGH2 user's guide, Version 2. Lawrence Berkeley National Laboratory Report LBNL-43134.

Shi, H., Holmes, J.A., Durlofsky, L.J., Aziz, K., Diaz, L.R., Alkaya, B., Oddie, G., (2005). Drift-flux modeling of two-phase flow in wellbores. *SPE Journal 10*, pp. 24–33.

Theis, C.V.: The relation between the lowering of the piezometric surface and the rate and duration of discharge of a well using ground water storage. *Transactions, American Geophysical Union 16*, 2, pp. 519–524. (1935).

Tonkin, R.A., O'Sullivan, M.J., O'Sullivan, J.P., (2021). A review of mathematical models for geothermal wellbore simulation. *Geothermics 97*, 102255.

Tonkin, R., O'Sullivan, J., Gravatt, M., O'Sullivan, M., (2023a). Simulation of complex transient flows in geothermal wells. *Geothermics 108*, 102631.

Tonkin, R., O'Sullivan, J., Gravatt, M., O'Sullivan, M., (2023b). A transient geothermal wellbore simulator. *Geothermics 110*, 102653.

ISSN 2703-4275